INTERNATIONAL JOURNAL OF
NUMERICAL ANALYSIS AND MODELING
Volume 14, Number 3, Pages 405–418

PRICING EUROPEAN OPTIONS ON ZERO-COUPON BONDS WITH A FITTED FINITE VOLUME METHOD

KAI ZHANG AND XIAO QI YANG

Abstract. We present a novel numerical scheme to price European options on discount bond, where the single factor models are adopted for the short interest rate. This method is based on a fitted finite volume (FFVM) scheme for the spatial discretization and an implicit scheme for the time discretization. We show that this scheme is consistent, stable and monotone, hence it ensures the convergence to the solution of continuous problem. Numerical experiments are performed to verify the effectiveness and usefulness of this new method.

Key words. Option pricing, finite volume method, partial differential equation.

1. Introduction

Interest rate derivatives, like bond options, range notes, interest rate caps, swaps and swaptions, are commonly traded in the financial markets. A large number of attention have been given to the development of models to price and hedge these types of derivatives. While the Black and Scholes [4] model has been well-known as the model for stock derivatives, many approaches to modeling interest rate derivatives are simultaneously established among academics and practitioners, such as Black-Karasinski model [3], Vasicek model, CIR model, HW model [9, 13, 6], Brennan-Schwartz model [5], and so on. Compared to stock derivatives, the pricing and hedging of interest rate derivatives pose greater challenges. For instance, for a simple bond option, unlike stock derivatives, its underlying asset is a bond whose price is dependent on interest rate and time. It is thus necessary to develop dynamic models that describe the stochastic evolution of the whole yield curve, which makes pricing interest rate derivatives a complex task.

In this paper, we focus on pricing European options on zero-coupon bonds under the single factor models. In [10, 6, 13], the price of this type of options has been investigated. Usually, this problem is formulated as a parabolic partial differential equation (PDE) with suitable boundary and terminal conditions [10]. In some simple cases, analytical solutions are available. However, these analytical solution usually is not easily computable [13]. Moreover, in most practical situations (for instance, path-dependent options) analytical solutions are unavailable. Hence, numerical solutions are normally sought for pricing bond options. Lattice method and the usual finite difference method are commonly used to pricing stock options. Unfortunately, it is pointed out in [14] and [1] that these methods are only convergent for certain combination of parameters.

The fitted finite volume method was first used to price the standard European stock options in [16], then generalized to other types of options, see [8, 18], etc. The method is based on a popular exponentially fitting technique widely used for problems with boundary and interior layers (cf. [11, 12]). It has been shown that this method makes greater success in pricing stock options, where the standard Black-Scholes equations are applied. It is easy to see that the PDE resulted from

Received by the editors December 23, 2015.
2000 *Mathematics Subject Classification.* 91G60, 65M12, 65M60.

European option model is degenerate and convection-dominated, hence the fitted finite volume method is a natural way to overcoming these difficulties. Its success motivates us to generalize the fitted finite volume technique to price bond options. On this basis, in this paper we derive a novel fitted finite volume method to price European bond options. We then apply this new fitted finite volume scheme in space with the implicit scheme in time to numerical valuation of European options on a discount bonds under single factor models. To guarantee the convergence of this new numerical scheme, we show that this numerical scheme is consistent, stable and monotone, hence convergent. To verify the accuracy and robustness of the new numerical scheme, some numerical experiments including a vanilla European option and a digital option on a discount bond under CIR model are implemented. Moreover, to testify its effectiveness a vanilla European option on a discount bond under a mean-reverting lognormal model is investigated. These numerical results show that this numerical scheme is very accurate, efficient and robust.

The paper is organized as follows. In the next section, the mathematical model for European options on a discount bond is presented. Then, the fitted finite volume method is developed in Section 3. In Section 4, the full discrete scheme is proposed and by showing the stability and monotonicity of this numerical scheme, its convergence is investigated. Finally, in the last section three numerical examples are given to illustrated the convergence and robustness of this numerical scheme.

2. Mathematical model for options on a zero-coupon bond

In this paper, we assume the following single factor model is applied for the interest rate term structure. That means the short-term interest rate r is governed by a stochastic process of the form.

$$dr = A(r,t)\,dt + \sigma r^{\xi} dW, \tag{1}$$

where dW is the increment of a Wiener process, $A(r,t)$ is the instantaneous drift, σr^{ξ} is the instantaneous volatility. Some well known-examples of one-factor interest rate models are special cases of Equation (1). Particularly, if $A(r,t)$is specified to be mean-reverting and independent of time t, and σ is a constant, the setting $\xi = 0, 1/2, 1, 3/2$ produces the Vasicek model, CIR model, lognormal model and cubic variance model, respectively.

Now, let $P(r,t,s)$ be the price of a pure discount bond with face value \$1 at its maturity date s. Based on the standard no-arbitrage pricing arguments, the bond price is governed by the following parabolic partial differential equation (PDE) [17]:

$$-\frac{\partial P}{\partial t} = \frac{1}{2}\sigma^2 r^{2\xi}\frac{\partial^2 P}{\partial r^2} + \left(A(r,t) + \sigma\lambda(r,t)\, r^{\xi}\right)\frac{\partial P}{\partial r} - rP, \tag{2}$$

where $\lambda(r,t) \geq 0$ is called the market price of risk. At the maturity date s the price of a pure discount bond is its face value, i.e.

$$P(r, t = s, s) = 1.$$

The boundary conditions are usually given by the following form

$$\begin{aligned} P(0,t,s) &= g_0(r,t), \qquad r \to 0, \\ P(r,t,s) &= 0, \qquad r \to \infty, \end{aligned}$$

where $g_0(r,t)$ can be determined according to different interest rate models.

Let $V(r,t)$ denote the value of an European option on a pure discount bond with striking price K,where the holder can receive the payoff $V^*(r,T)$ at expiry date T.

It is known that the value $V(r,t)$ is also governed by the same type of PDE as (2), i.e.

$$-\frac{\partial V}{\partial t}=\frac{1}{2}\sigma^2 r^{2\xi}\frac{\partial^2 V}{\partial r^2}+\left(A(r,t)+\sigma\lambda(r,t)\,r^{\xi}\right)\frac{\partial V}{\partial r}-rV. \tag{3}$$

At $t=T$, we set $V(r,T)$ to the specified contract payoff, i.e.

$$V(r,t=T)=V^*(r,T)=\begin{cases}\max\left[P(r,T,s)-K,0\right], & \text{for a call,}\\ \max\left[K-P(r,T,s),0\right], & \text{for a put.}\end{cases}$$

The boundary conditions are given by the following form

$$V(0,t)=g_1(r,t), \qquad r\to 0, \tag{4}$$

$$V(r,t)=g_2(r,t), \qquad r\to\infty, \tag{5}$$

where $g_1(r,t)$ and $g_2(r,t)$ can be determined by financial reasoning. For computational purpose, we restrict r in a region $I=[0,R]$, where R is sufficiently large to ensure the accuracy of the solution ([17]). Thus, (5) becomes

$$V(R,t)=g_2(R,t). \tag{6}$$

Remark 2.1. *In the case of pricing vanilla European options on zero-coupon bonds, there are several ways to determine the boundary conditions (4) and (6), see* [15] *and the references therein. A popular and simple choice is as follows* [7]*:*

$$V(r=0,t)=\begin{cases}\max\left[P(0,t,s)-KP(0,t,T),0\right], & \textit{for a call,}\\ 0, & \textit{for a put,}\end{cases}$$

$$V(r=R,t)=\begin{cases}0, & \textit{for a call,}\\ \max\left[KP(R,t,T)-P(R,t,s),0\right], & \textit{for a put.}\end{cases}$$

Remark 2.2. *It is worth noting that $T<s$ and $K<P(0,T,s)=A(T,s)$ for a call option or $K>A(T,s)$ for a put option, since otherwise the option would never be exercised and would be worthless.*

3. The fitted finite volume method

Since the bond pricing equation (2) has the same form with European bond option pricing equation (3), in this section we will present the fitted finite volume discretization of (3). Before proceeding to the discretization scheme, we first transform (3), (4) and (6) into the following conservative form:

$$\frac{\partial V}{\partial \tau}=\frac{\partial}{\partial r}\left[ar^{2\xi}\frac{\partial V}{\partial r}+b(r,\tau)\,V\right]-c(r,\tau)\,V, \tag{7}$$

where $\tau=T-t$ and

$$\begin{aligned}a&\equiv a(r,\tau)=\sigma^2/2,\\ b(r,\tau)&=\left(A(r,\tau)+\sigma\lambda(r,\tau)\,r^{\xi}\right)-2a\xi r^{2\xi-1},\\ c(r,\tau)&=r+\frac{\partial b}{\partial r}.\end{aligned} \tag{8}$$

The fitted finite volume method is based on the self-adjoint form (7). We first define two space partitions of I. Let I be divided into N sub-intervals

$$I_i=(r_i,r_{i+1}), \quad i=0,\ldots,N-1,$$

with $0=r_0<r_1<\cdots<r_N=R$. For each $i=0,\ldots,N-1$, let $h_i=r_{i+1}-r_i$. Also, we let $r_{i-1/2}=(r_{i-1}+r_i)/2$ and $r_{i+1/2}=(r_i+r_{i+1})/2$ for each $i=2,\ldots,N$. These intervals $J_i=(r_{i-1/2},r_{i+1/2})$ form a second partition of $I=[0,R]$ if we define $r_{-1/2}=r_0$ and $r_{N+1/2}=r_{N+1}$.

For each $i = 1, \ldots, N-1$, integrating (7) over J_i, we have

$$\int_{J_i} \frac{\partial V}{\partial \tau} dr = \left[r^{2\xi-1} \left(ar \frac{\partial V}{\partial r} + br^{1-2\xi} V \right) \right]_{r_{i-1/2}}^{r_{i+1/2}} - \int_{J_i} cV dr. \tag{9}$$

Applying the one-point quadrature rule to all the terms in (9) except the first term in the right hand side, we obtain

$$\frac{\partial V_i}{\partial \tau} l_i = \left[r_{i+1/2}^{2\xi-1} \rho(V)|_{r_{i+1/2}} - r_{i-1/2}^{2\xi-1} \rho(V)|_{r_{i-1/2}} \right] - c_i l_i V_i, \tag{10}$$

for $i = 1, \ldots, N-1$, where $l_i = r_{i+1/2} - r_{i-1/2}$ is the length of interval J_i, $c_i = c(r_i, \tau)$, V_i denotes the nodal approximation to $V(r_i, \tau)$ to be determined and $\rho(V)$ is the weighted flux density associated with V defined by

$$\rho(V) := arV' + d(r) V, \tag{11}$$

where $d(r, \tau) = b(r, \tau) r^{1-2\xi}$.

We now derive the approximation of the continuous flux $\rho(V)$ defined above at the mid-point, on $r_{i+1/2}$, of the interval I_i for all $i = 0, \ldots, N-1$. Consider the following two-point boundary value problem:

$$\begin{array}{l} \left(arV' + d_{i+1/2} V \right)' = 0, \quad r \in I_i, \\ V(r_i) = V_i, \ V(r_{i+1}) = V_{i+1}, \end{array} \tag{12}$$

where $d_{i+1/2} = d\left(r_{i+1/2}, \tau\right)$. Solving this equation analytically, we obtain

$$\rho_i(V) = d_{i+1/2} \frac{r_{i+1}^{\eta_i} V_{i+1} - r_i^{\eta_i} V_i}{r_{i+1}^{\eta_i} - r_i^{\eta_i}}, \tag{13}$$

where

$$\eta_i = d_{i+1/2}/a. \tag{14}$$

Similarly, we can define the approximation of the flux at $r_{i-1/2}$.

Note that the above analysis does not apply to the approximation to the flux on $I_0 = (0, r_1)$, because (12) is degenerated. To overcome this difficulty, we reconsider (12) with an extra degree freedom in the following form:

$$\begin{array}{ll} \left(arV' + d_{1/2} V \right)' = C, & r \in I_0, \\ V(0) = V_0, & V(r_1) = V_1. \end{array} \tag{15}$$

Solving this local problem analytically, we have

$$\begin{aligned} \rho_0(V) = \left(arV' + d_{1/2} V \right)_{r_{1/2}} &= \frac{1}{2} [(a + d_{1/2}) V_1 - (a - d_{1/2}) V_0], \\ V = V_0 + (V_1 - V_0) r/r_1, &\qquad r \in I_0 = (0, r_1). \end{aligned} \tag{16}$$

Now using (13) and (16), we define a global piecewise constant approximation to $\rho(V)$ by $\rho_h(V)$ satisfying

$$\rho_h(V) = \rho_i(V), \quad \text{if } r \in I_i \tag{17}$$

for $i = 0, \ldots, N-1$.

Substituting (13) and (16) into (10), we have the following semi-discretization

$$\frac{\partial V_i}{\partial \tau} = \alpha_i V_{i-1} + \gamma_i V_i + \beta_i V_{i+1}, \tag{18}$$

for $i = 1, \ldots, N-1$, where

$$\begin{aligned}
\alpha_1 &= \frac{r_1^{2\xi-1}}{2l_1}\left(a - d_{1/2}\right), \\
\beta_1 &= \frac{b_{3/2} r_2^{\eta_1}}{\left(r_2^{\eta_1} - r_1^{\eta_1}\right) l_1}, \\
\gamma_1 &= -\frac{r_1^{2\xi-1}}{2l_1}\left(a + d_{1/2}\right) - \frac{b_{3/2} r_1^{\eta_1}}{\left(r_2^{\eta_1} - r_1^{\eta_1}\right) l_1} - c_1,
\end{aligned}$$

and

$$\begin{aligned}
\alpha_i &= \frac{b_{i-1/2} r_{i-1}^{\eta_{i-1}}}{\left(r_i^{\eta_{i-1}} - r_{i-1}^{\eta_{i-1}}\right) l_i}, \\
\beta_i &= \frac{b_{i+1/2} r_{i+1}^{\eta_i}}{\left(r_{i+1}^{\eta_i} - r_i^{\eta_i}\right) l_i}, \\
\gamma_i &= -\frac{b_{i-1/2} r_i^{\eta_{i-1}}}{\left(r_i^{\eta_{i-1}} - r_{i-1}^{\eta_{i-1}}\right) l_i} - \frac{b_{i+1/2} r_i^{\eta_i}}{\left(r_{i+1}^{\eta_i} - r_i^{\eta_i}\right) l_i} - c_i,
\end{aligned} \tag{19}$$

for $i = 2, \ldots, N-1$. These forms an $(N-1)\times(N-1)$ linear system for $[V_1, V_2, \ldots V_{N-1}]$ with V_0 and V_n being equal to the given boundary conditions in (4) and (6).

4. Full discretization and its convergence

4.1. Full discretization. Let's now consider the time discretization of (18). Let $\tau_i \ \ (i = 0, \ldots, M)$ be a set of portion points in $[0, T]$ satisfying $0 = \tau_0 < \tau_1 < \ldots < \tau_M = T$ with the time step sizes $\Delta\tau_n = \tau_n - \tau_{n-1} > 0$, where $M > 1$ is a positive integer. There are several implicit schemes we can use. For example, the first-order fully implicit method and the second-order Crank-Nicolson method. For discussion simplicity, we apply the fully implicit scheme to (18), yielding

$$\frac{V_i^{n+1} - V_i^n}{\Delta\tau_{n+1}} = \alpha_i V_{i-1}^{n+1} + \gamma_i V_i^{n+1} + \beta_i V_{i+1}^{n+1}, \tag{20}$$

where $V_i^n = V\left(r_i, \tau_n\right)$ denotes the solution at node r_i and time level τ_n. If we define

$$\begin{aligned}
V^n &= [V_1^n, \cdots, V_{N-1}^n]^\top, \\
R^n &= [\alpha_1 V_0^n, 0, \cdots 0, \beta_{N-1} V_N^n]_{N-1}^\top,
\end{aligned}$$

and

$$M = \begin{bmatrix}
\gamma_1 & \beta_1 & & & \\
\alpha_2 & \gamma_2 & \beta_2 & & \\
& \ddots & \ddots & \ddots & \\
& & \alpha_{N-1} & \gamma_{N-1}
\end{bmatrix}_{(N-1)\times(N-1)}.$$

Then, we can write (20) as the following equivalent matrix form,

$$\frac{V_i^{n+1} - V_i^n}{\Delta\tau_{n+1}} = \left[MV^{n+1} + R^n\right]_i. \tag{21}$$

It should be noted that in (21) the boundary conditions at $r = 0$ and $r = r_{max}$ have been incorporated, where the Dirichlet types boundary solution is applied for specific option types as defined in (4) and (6). Also, the initial condition is incorporated as the payoff function given for the specific option type.

For the numerical scheme (21), we establish the following result.

Theorem 4.1. *Both $-M$ and $I-\Delta\tau_{n+1}M$ are M-matrices, provided that $r>0$ and $l_i\to 0$.*

Proof. Let us first investigate α_i and β_i. We have

$$-\alpha_i\le 0, -\beta_i\le 0. \tag{22}$$

This is because it follows from (8) and (14) that

$$\begin{aligned}
-\alpha_i &= \frac{b_{i-1/2}r_{i-1}^{\eta_{i-1}}}{\left(r_i^{\eta_{i-1}}-r_{i-1}^{\eta_{i-1}}\right)l_i} = -\frac{d_{i-1/2}r_{i-1}^{\eta_{i-1}}r_{i-1/2}^{2\xi-1}}{\left(r_i^{\eta_{i-1}}-r_{i-1}^{\eta_{i-1}}\right)l_i}\\
&= \frac{-a\eta_i}{r_i^{\eta_i}-r_{i-1}^{\eta_i}}\left(\frac{r_{i-1}^{\eta_{i-1}}r_{i-1/2}^{2\xi-1}}{l_i}\right)\\
&= -\frac{\eta_i}{r_i^{\eta_i}-r_{i-1}^{\eta_i}}\left(\frac{\sigma^2}{2}\frac{r_{i-1}^{\eta_{i-1}}r_{i-1/2}^{2\xi-1}}{l_i}\right)\\
&\le 0,
\end{aligned}$$

for all $i=2,3,\dots N-1$,since $\sigma>0, r_i>r_{i-1}\ge 0, l_i>0$ and $\frac{\eta_i}{r_i^{\eta_i}-r_{i-1}^{\eta_i}}>0$. In the same way, we also get $-\beta_i\le 0$.

On the other hand, it follows from (19), (8) and the Taylor expansions of $b_{i-1/2}$ and $b_{i+1/2}$ at r_i that

$$\begin{aligned}
-\alpha_i-\beta_i-\gamma_i =& -\frac{b_{i-1/2}r_{i-1}^{\eta_{i-1}}}{\left(r_i^{\eta_{i-1}}-r_{i-1}^{\eta_{i-1}}\right)l_i}-\frac{b_{i+1/2}r_{i+1}^{\eta_i}}{\left(r_{i+1}^{\eta_i}-r_i^{\eta_i}\right)l_i}\\
&+\frac{b_{i-1/2}r_i^{\eta_{i-1}}}{\left(r_i^{\eta_{i-1}}-r_{i-1}^{\eta_{i-1}}\right)l_i}+\frac{b_{i+1/2}r_i^{\eta_i}}{\left(r_{i+1}^{\eta_i}-r_i^{\eta_i}\right)l_i}+c_i\\
=&\frac{1}{l_i}\left[b_{i-1/2}-b_{i+1/2}\right]+c_i\\
=&\frac{1}{l_i}\left[b_{i-1/2}-b_{i+1/2}\right]+r_i+\frac{\partial b_i}{\partial r}\\
=&\frac{1}{l_i}\left[-\frac{\partial b_i}{\partial r}l_i+o\left(l_i^3\right)\right]+r_i+\frac{\partial b_i}{\partial r}\\
=&r_i+o\left(l_i^2\right)\ge 0,
\end{aligned} \tag{23}$$

given that $r>0$ and $l_i\to 0$. Thus,

$$-\gamma_i=r_i+\alpha_i+\beta_i+o\left(l_i^2\right)\ge 0,\quad \text{as } l_i\to 0 \tag{24}$$

Summarizing (22), (23) and (24), we conclude that $-M$ has non-positive off-diagonals, positive diagonals, and is diagonally dominant. Hence, $-M$ is an M-matrix. Consequently, $I-\Delta\tau_{n+1}M$ is also an M-matrix. □

Remark 4.1. *Theorem 4.1 implies that the fully discrete system (21) satisfies the discrete maximum principle. This guarantees that the discrete arbitrage inequality holds, which is an important property in option pricing theory.*

4.2. Convergence of the numerical scheme (21). In this subsection, we investigate the convergence property of scheme (21). As the pricing equation (3) is degenerate and convection-dominated with nonsmooth boundary conditions, it is important to ensure that we generate a numerical solution which is guaranteed to converge to its corresponding continuous solution, i.e viscosity solution [2]. It has been shown in [2] that the solution of the discrete system (21) will converge to the

viscosity solution if the discretization is consistent, stable and monotone. Thus, we will show that this numerical scheme satisfies these conditions.

For convenience, let

$$h = \max\left\{\max_i \Delta r_i, \max_n \Delta\tau_n\right\},$$

be the mesh parameter, where $\Delta r_i = (r_i - r_{i-1})$ and $\Delta\tau_n = (\tau_n - \tau_{n-1})$. Assume the partition is quasi-uniform, i.e. $\exists C_1, C_2 > 0$ independent of h, such that

$$C_1 h \le \Delta r_i, \Delta\tau_n \le C_2 h,$$

for $0 \le i \le N$ and $0 \le n \le M$. With these notations, we can write (21) in the following component form:

$$F_i^{n+1}(h, V_i^{n+1}, V_{i+1}^{n+1}, V_{i-1}^{n+1}, V_i^n) = 0,$$

where

$$F_i^{n+1} = \left[(I - \Delta\tau_{n+1}M)\, V^{n+1}\right]_i - V_i^n - \Delta\tau_{n+1}R_i^n. \tag{25}$$

First, we have the following consistency result for the numerical scheme (21).

Lemma 4.1. *[Consistency]The discretization (21) is consistent.*

Proof. From the discretization in Section 2, we can see that the consistency of scheme (21) relies on the consistency of the flux $\rho(V)$. Let w be a sufficiently smooth function and let w_h be the discrete approximation of w. From (11) and (17), it is easy to see that the exact and the discrete flux yield

$$\begin{aligned}\left|[\rho(w) - \rho_h(w_h)]_{r_{i+1/2}}\right| &\le \left|[\rho(w) - \rho(w_h) + \rho(w_h) - \rho_h(w_h)]_{r_{i+1/2}}\right| \\ &\le \left|[\rho(w) - \rho(w_h)]_{r_{i+1/2}}\right| + \left|[\rho(w_h) - \rho_h(w_h)]_{r_{i+1/2}}\right| \\ &\le \left|d - d_{i+1/2}\right| \cdot \left|w_{i+1/2}\right| + \left|[\rho(w_h) - \rho_h(w_h)]_{r_{i+1/2}}\right|.\end{aligned}$$

From (12), we see that the mapping from $\rho(w)$ to $\rho_h(w_h)$ preserve constants. Therefore, by a standard arguments we obtain

$$\left|[\rho(w_h) - \rho_h(w_h)]_{r_{i+1/2}}\right| \le Ch.$$

Summarizing the above two inequalities, we eventually have the consistency of the flux

$$\left|[\rho(w) - \rho_h(w_h)]_{r_{i+1/2}}\right| \le Ch.$$

Hence, the consistency of the discretization (21) is a consequent result. □

The stability result for the numerical scheme is given as below.

Lemma 4.2. *[Stability] The discretization (21) is stable, i.e.*

$$\|V^n\|_\infty \le \max(\|V^0\|_\infty, C_3, C_4), \tag{26}$$

where $C_3 = \max_n |V_0^n|$ and $C_4 = \max_n |V_N^n|$, with V_0^n and V_N^n being the given Dirichlet boundary conditions.

Proof. It follows from (20), (22)-(24) that

$$\begin{aligned}(1 - \Delta\tau_{n+1}\gamma_i^{n+1})|V_i^{n+1}| &\le |V_i^n| + \Delta\tau_{n+1}\alpha_i^{n+1}|V_{i-1}^{n+1}| + \Delta\tau_{n+1}\beta_i^{n+1}|V_{i+1}^{n+1}| \\ &\le \|V^n\|_\infty + \|V^{n+1}\|_\infty(\alpha_i^{n+1} + \beta_i^{n+1})\Delta\tau_{n+1}. \qquad (27)\end{aligned}$$

If $\|V^{n+1}\|_\infty = |V_j^{n+1}|, 0 < j < N$, then (27) becomes

$$(1 - \Delta\tau_{n+1}\gamma_j^{n+1})\|V^{n+1}\|_\infty \le \|V^n\|_\infty + \|V^{n+1}\|_\infty(\alpha_j^{n+1} + \beta_j^{n+1})\Delta\tau_{n+1}.$$

Thus, from (22) we obtain

$$\|V^{n+1}\|_\infty \le \frac{\|V^n\|_\infty}{1-\Delta\tau_{n+1}(\alpha_j^{n+1}+\beta_j^{n+1}+\gamma_j^{n+1})} = \frac{\|V^n\|_\infty}{1+r\Delta\tau_{n+1}} \le \|V^n\|_\infty. \tag{28}$$

If $j = 0$ or N, then

$$\|V^{n+1}\|_\infty = |V_0^{n+1}|, \text{ or } \|V^{n+1}\|_\infty = |V_N^{n+1}|. \tag{29}$$

Combining (28) and (29) gives

$$\|V^{n+1}\|_\infty \le \max(\|V^0\|_\infty, |V_0^{n+1}|, |V_N^{n+1}|),$$

which then results in (26). Hence the discretization (21) is stable. □

Finally, we have the following monotonicity result for the scheme (21).

Lemma 4.3. *[Monotonicity] The discretization (21) is unconditionally monotone, i.e., for any $\epsilon > 0$, and $i = 0, 1, \cdots, N$*

$$\begin{aligned} &F_i^{n+1}(h, V_i^{n+1}, V_{i+1}^{n+1}+\epsilon, V_{i-1}^{n+1}+\epsilon, V_i^n+\epsilon) \\ &\quad \le F_i^{n+1}(h, V_i^{n+1}, V_{i+1}^{n+1}, V_{i-1}^{n+1}, V_i^n), \\ &F_i^{n+1}(h, V_i^{n+1}+\epsilon, V_{i+1}^{n+1}, V_{i-1}^{n+1}, V_i^n) \\ &\quad \ge F_i^{n+1}(h, V_i^{n+1}, V_{i+1}^{n+1}, V_{i-1}^{n+1}, V_i^n). \end{aligned} \tag{30}$$

Proof. For $i = 0$ or N, the lemma is trivially true. When $0 < i < N$, the component form (25) of the scheme (21) is stated as

$$\begin{aligned} &F_i^{n+1}(h, V_i^{n+1}, V_{i+1}^{n+1}, V_{i-1}^{n+1}, V_i^n) \\ &= \left[(I-\Delta\tau_{n+1}M)\,V^{n+1}\right]_i - V_i^n - \Delta\tau_{n+1}R_i^n, \end{aligned} \tag{31}$$

Now, we examine each term in (31). From Theorem 4.1, matrix $I - \Delta\tau_{n+1}M$ is an M-matrix, hence $\left[(I-\Delta\tau_{n+1}M)\,V^{n+1}\right]_i$ is a strictly increasing function of V_i^{n+1}, and non-increasing function of V_{i+1}^{n+1} and V_{i-1}^{n+1}. On the other hand, $-V_i^n$ is a decreasing function of V_i^n. Hence (30) is satisfied and the discretization (21) is monotone. □

The following theorem follows from the consistency, stability and monotonicity of the scheme (21).

Theorem 4.2. *The solution of the fully implicit scheme (21) converges to the continuous solution of (2), as $h \to 0$.*

5. Numerical experiments

In this section, we present some numerical tests to demonstrate the performance and convergence of the new numerical scheme. In particular, we investigate the effectiveness and accuracy of this numerical scheme. Firstly, a numerical test on European bond option under CIR model is under consideration, where $\xi = 1/2$ in (1) . It is known that in this case the analytical pricing formula is available. Hence, this test can be carried out to verify the accuracy of the new scheme. Secondly, a numerical example on a digital call option under CIR model is considered to test its robustness. Finally, to show the usefulness of the new scheme a European option under a lognormal interest rate model, where $\xi = 1$ in (1) and no analytical solution is available, is under investigation. Furthermore, we determine the numerical rates of convergence as well. To do so, we choose a sequence of meshes by successively halving the mesh parameters. When an analytical solution exists, we use it as the 'exact solution'. Otherwise, we use the solution on the best mesh as the 'exact

TABLE 1. Data used to value European options on a zero-coupon bond under CIR model.

Parameter values	
κ	0.10
θ	0.08
σ	0.50
λ	0
E	100
K	60
T	1
s	5

solution'. Then, we compute the following ratios of the numerical solutions of the consecutive meshes:

$$\text{Ratio}(\|\cdot\|_{h,\infty}) = \frac{\left\|V^h_{\Delta\tau} - V\right\|_{h,\infty}}{\left\|V^{h/2}_{\Delta\tau/2} - V\right\|_{h,\infty}} \tag{32}$$

in the solution domain, where V^β_α denotes the computed solution on the mesh with spatial mesh β and time mesh size α.

$$\left\|V^h_{\Delta\tau} - V\right\|_{h,\infty} := \max_{1\le i\le N; 1\le n\le M} \left|V^n_i - V(r_i,\tau_n)\right|.$$

The numerical order of convergence is then defined by

$$\text{Rate} = \log_2 \text{Ratio}.$$

All the numerical experiments were carried out with Matlab 2008a on a P4 3.0GHz Intel PC.

5.1. European option under CIR model. A vanilla call option on zero-coupon bond has the payoff

$$V^* = \max\left[P(r,T,s) - K, 0\right],$$

The parameters used for this call option on bond under CIR model are listed in Table 1.

For the call option on bond with the parameters in Table 1, we choose $r_{max} = 2$ to ensure the desirable accuracy. The coarsest grid is defined as $h = 0.01$ and $\Delta\tau = 0.01$, uniformly.

In this numerical experiment, the ratio is computed at all the space and time steps. Table 2 gives the results computed by the fitted finite volume method with the implicit time scheme, where N_r and N_τ represent the number of space steps and time steps, respectively; Ratio is defined in (32); CPU represents the CPU time in second. The 'exact solution' is computed by the following analytical result [13]:

$$\begin{aligned} V(r,t) = \;& P(r,t,s)\,\chi^2\left(2r^*\left[\phi+\psi+B(T,s)\right]; \tfrac{4\kappa\theta}{\sigma^2}, \tfrac{2\phi^2 r e^{\gamma(T-t)}}{\phi+\psi+B(T,s)}\right) \\ & -KP(r,t,T)\,\chi^2\left(2r^*\left[\phi+\psi\right]; \tfrac{4\kappa\theta}{\sigma^2}, \tfrac{2\phi^2 r e^{\gamma(T-t)}}{\phi+\psi}\right). \end{aligned}$$

where χ^2 is the non-central chi-squared distribution and

$$\begin{aligned} &\gamma = \left(\kappa+\lambda+2\sigma^2\right)^{1/2}, \quad \phi = \tfrac{2\gamma}{\sigma^2\left(e^{\gamma(T-t)}-1\right)}, \\ &\psi = \tfrac{(\kappa+\lambda+\gamma)}{\sigma^2}, \qquad\qquad r^* = \tfrac{\ln(A(T,s)/K)}{B(T,s)}. \end{aligned} \tag{33}$$

TABLE 2. Result of an European call option on a zero-coupon bond under CIR model using the fitted finite volume method combined with the implicit scheme, data as in Table 1.

N_r	N_τ	$\|\cdot\|_{h,\infty}$	Ratio($\|\cdot\|_{h,\infty}$)	CPU
201	100	0.1794		$0.015s$
401	200	0.1062	1.7	$0.029s$
801	400	0.0640	1.7	$0.054s$
1601	800	0.0364	1.8	$0.159s$
3201	1600	0.0162	2.2	$0.576s$
6401	3200	0.0077	2.1	$2.893s$

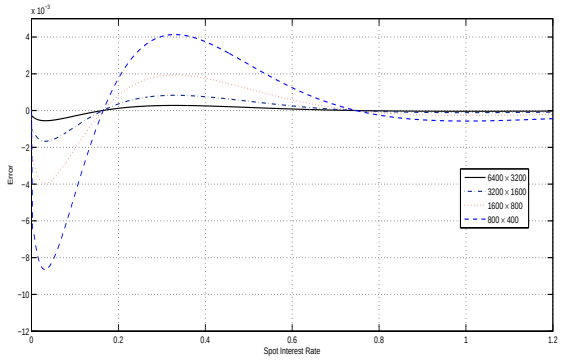

FIGURE 1. Errors at the last time step of the call option with different mesh grids, where the fitted finite volume method combined with the implicit scheme is used, data as in Table 1. $N_r \times N_\tau$ represents the number of space steps times the number of time steps.

Finally, we plot, in Figure 1, the error at the last time step of this option with different mesh girds.

5.2. Digital option under CIR model. Now, we choose a digital call option to test our numerical scheme. A digital call option has the discontinuous payoff

$$V(r, \tau = 0) = \begin{cases} 1, & \text{if } P(r, T, s) \geq K, \\ 0, & \text{if } P(r, T, s) < K. \end{cases}$$

We choose the same parameters defined in Table 1 for this digital call option. We also choose the coarsest grid as $h = 0.01$ and $\Delta\tau = 0.01$, uniformly. The ratio is computed at all the space and time steps. Table 3 gives the results computed by the fitted finite volume method with the implicit time scheme. The notations in Table 3 is defined as the same with those in the first example. The 'exact solution' is computed on the uniform mesh with 12801×6400 nodes.

Finally, we plot, in Figure 2, the value of the digital call option on a zero-coupon bond.

5.3. European option under lognormal interest rate model. As a final example, we choose a European call option under lognormal interest rate model to show the usefulness of our numerical scheme. Unlike the CIR model, no closed-form solutions are available for both pure discount bond price and bond option price.

TABLE 3. Result of a digital call option on a zero-coupon bond under CIR model using the fitted finite volume method combined with the implicit scheme, data as in Table 1.

N_r	N_τ	$\|\cdot\|_{h,\infty}$	Ratio($\|\cdot\|_{h,\infty}$)	CPU
201	100	0.01469		$0.020s$
401	200	0.01087	1.4	$0.031s$
801	400	0.00743	1.5	$0.065s$
1601	800	0.00379	2.0	$0.179s$
3201	1600	0.00197	1.9	$0.622s$
6401	3200	0.00104	1.9	$2.642s$

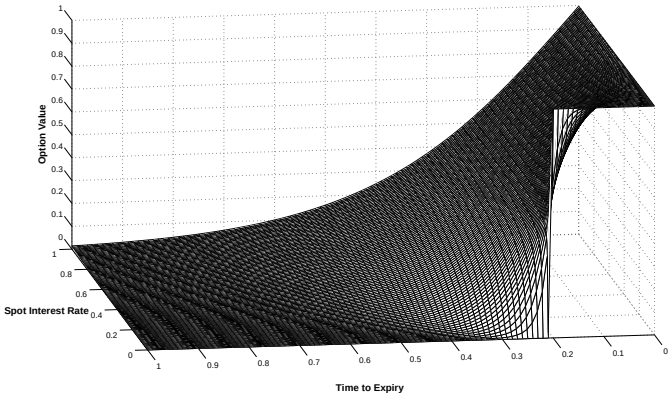

FIGURE 2. Digital call option value using the fitted finite volume method combined with the implicit scheme, data as in Table 1. Grid: $N_r = 201$, $N_\tau = 100$.

TABLE 4. Data used to value European options on a zero-coupon bond under lognormal interest rate model.

Parameter values	
κ	0.06
θ	0.03
σ	0.80
λ	0
E	100
K	60
T	1
s	5

Hence, we first need to price the bond price numerically and then use the numerical prices to compute the valuation of European options. The parameters used for this call option on bond under lognormal model are listed in Table 4.

TABLE 5. Results of a pure discount bond and a European option on this bond under lognormal interest rate model using the fitted finite volume method combined with the implicit scheme, data as in Table 4.

r	0.02	0.04	0.06	0.08	0.10	0.12	0.14	0.16	0.18	0.20
$P(r, t=0, s)$	90.56	84.36	78.97	74.22	69.96	66.11	62.61	59.41	56.46	53.74
$V(r, t=0)$	30.17	24.77	20.49	17.07	14.32	12.10	10.29	8.80	7.57	6.54

TABLE 6. Result of a European call option on a zero-coupon bond under lognormal interest rate using the fitted finite volume method combined with the implicit scheme, data as in Table 4.

N_r	N_τ	$\|\cdot\|_{h,\infty}$	Ratio($\|\cdot\|_{h,\infty}$)	CPU
501	100	0.02635		$0.030s$
1001	200	0.01895	1.4	$0.090s$
2001	400	0.01207	1.6	$0.232s$
4001	800	0.00678	1.8	$0.883s$
8001	1600	0.00376	1.8	$3.471s$
16001	3200	0.00221	1.7	$12.29s$

For this example, we choose $r_{max} = 5$ to ensure the desirable accuracy. Table 5 lists the bond prices and options prices on the uniform mesh with 32001×6400 nodes.

Table 6 gives the numerical convergence results computed by the fitted finite volume method with the implicit time scheme, where the coarsest grid $N_r \times N_\tau$ is set to 501×100, uniformly. The 'exact solution' is computed on the uniform mesh with 32001×6400 nodes.

Finally, we plot the values of the pure discount bond and the European call option on this bond in Figure 3.

In view of the results in Tables 2, 3 and 6, we can draw some desirable conclusions. Firstly, the columns '$\|\cdot\|_{h,\infty}$' in these tables clearly show a convergence trend. Furthermore, the columns 'Ratio' implies a linear convergence rate, which is consistent with the property of the fully implicit scheme. As we have proved in the previous sections, the fitted finite volume method combined with the fully implicit scheme is a consistent, stable and monotonic numerical scheme. Hence, the option values in these tables converge to their corresponding continuous solution. Secondly, the computed results in Tables 2 and 3 show this new numerical scheme is fast and robust. Especially, for the digital call option on bond where a boundary layer exits, Figure 2 shows that the numerical solution from our method is qualitatively very good and contains no oscillations or kinks. It shows that the fitted finite volume method combined with the implicit scheme is robust. Finally, Table 5 and Figure 3 clearly show that the new scheme is quite effective and robust when the interest rate follows a lognormal model.

6. Conclusion

In this work we developed a novel fitted finite volume method for the spatial discretization of the PDE arising from pricing European bond options. The method is coupled with a fully implicit time-stepping scheme. We have shown that the discretization scheme is consistent, stable and monotonic, hence the convergence is guaranteed. Numerical experiments were performed by using three models to

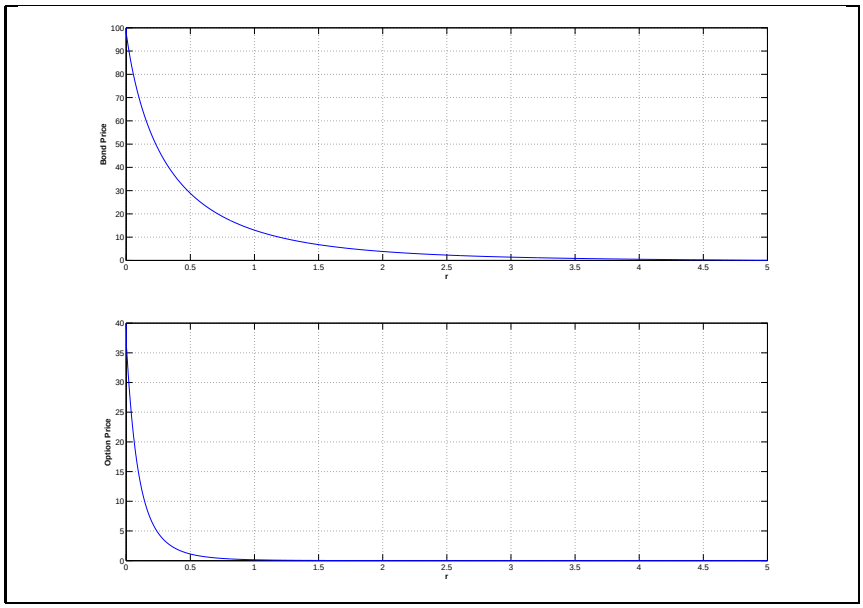

FIGURE 3. Bond price (top) and option price (bottom) at the last time step, where the fitted finite volume method combined with the implicit scheme is used, data as in Table 4.

demonstrate the convergence, efficiency and usefulness of this method. The numerical results show that the method is stable and the rate of convergence is of approximate 1st-order.

Acknowledgement

The authors would like to thank one anonymous referee for his/her helpful comments and suggestions toward the improvement of this paper. This work was supported by Philosophy and Social Science Program of Guangdong Province (Grant No. GD13YYJ01) and supported by the MOE Project of Key Research institute of Humanities and Social Sciences at Universities (Grant No. 14JJD790041). Project 11001178 partially supported by National Natural Science Foundation of China. The second author was supported by PolyU internal grant G-YBCN.

References

[1] W. Allegretto, Y. Lin and H. Yang, Numerical pricing of American put options on zero-coupon bonds, Applied Numerical Mathematics 46 (2003) 113-134.
[2] G. Barles, Convergence of numerical schemes for degenerate parabolic equations arising in finance. In L. C. G. Rogers, & D. Talay (Eds.), Numerical methods in finance (1st ed.), Cambridge: Cambridge University Press,1997.
[3] F. Black and P. Karasinski, Bond and option pricing when short rates are lognormal, Financial Analysts Journal, 47 (1991) 52-59.
[4] F. Black and M. Scholes, The pricing of options and corporate liabilities, J. Political Economy, 81 (1973) 637-659.
[5] G. Courtadon, The pricing of options on default-free bonds, Journal of Financial and Quantitative Analysis, XVII (1982), 75-100.
[6] J.C. Cox, J.E. Ingersoll and S.A. Ross, A theory of the term structure of interest rates, Econometrica 53 (1985) 385-407.
[7] G. Fusai, A. Roncoroni, Implementing models in quantitative finance: methods and cases, Springer-Verlag Berlin, Heidelberg, 2008.

[8] C.-S. Huang, C.-H. Hung and S. Wang, A fitted finite volume method for the valuation of options on assets with stochastic volatilities, Computing, 77 (2006) 297-320.
[9] J. Hull, Options, Futures, and Other Derivatives, Prentice-Hall, Englewood Cliffs, 2005.
[10] Y.K. Kwok, Mathematical Models of Financial Derivatives, Springer, Berlin, 1998.
[11] J.J.H. Miller and S. Wang, A new non-conforming Petrov-Galerkin method with triangular elements for a singularly perturbed advection-diffusion problem. IMA J. Numer. Anal., 14 (1994) 257-276.
[12] J.J.H. Miller and S. Wang, An exponentially fitted finite element volume method for the numerical solution of 2D unsteady incompressible flow problems. J. Comput. Phys., 115 (1994) 56-64.
[13] R. Rebonato, Interest-rate Option Models: Understanding, Analyzing and using Models for Exotic Interest-rate Options, Wiley, Chicherster, 1996.
[14] Y. Tian, A simplified binomial approach to the pricing of interest-rate contingent claims, J. Fin. Engrg. 1 (1992) 14-37.
[15] K.R. Vetzal, Stochastic volatility, movements in short term interest rates, and bond option values, J. Banking Finance, 21 (1997) 169-196.
[16] S. Wang, A novel fitted finite volume method for the Black-Scholes equation governing option pricing, IMA J. Numer. Anal., 24 (2004) 699-720.
[17] P. Wilmott, Paul Wilmott on Quantitative Finance, Wiley, New York, 2000.
[18] K. Zhang and S. Wang, A computational scheme for uncertain volatility model in option pricing. Appl. Math. Comput.,59 (2009) 1754-1767.

College of Economics, Shenzhen University, Shenzhen, Guangdong, 518060, China.
E-mail: mazhangkai@gmail.com

Department of Applied Mathematics, The Hong Kong Polytechnic University, Kowloon, Hong Kong
E-mail: xiao.qi.yang@polyu.edu.hk